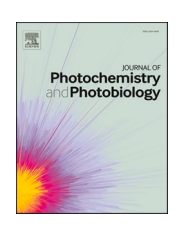
FISEVIER

Contents lists available at ScienceDirect

Journal of Photochemistry and Photobiology

journal homepage: www.sciencedirect.com/journal/journal-of-photochemistry-and-photobiology





Charge transfer vs. proton transfer in the excited-state dynamics of biomimetic pyranoflavylium cations

Eli M. Espinoza ^{a,1,2}, John A. Clark ^{b,1}, Cassio Pacheco da. Silva ^c, James B. Derr ^{d,3}, Gustavo Thalmer de Medeiros Silva ^c, Mimi K. Billones ^e, Maryann Morales ^{a,4}, Frank H. Quina ^c, Valentine I. Vullev ^{a,b,d,f,*}

- ^a Department of Chemistry, University of California, Riverside, CA 92521, USA
- ^b Department of Bioengineering, University of California, Riverside, CA 92521, USA
- c Instituto de Química, Universidade de São Paulo, Avenida Lineu Prestes 748, Cidade Universitária, São Paulo 05508-900, Brazil
- ^d Department of Biochemistry, University of California, Riverside, CA 92521, USA
- ^e Department of Biology, University of California, Riverside, CA 92521, USA
- f Materials Science and Engineering Program, University of California, Riverside, CA 92521, USA

ARTICLE INFO

Keywords: Pyranoflavylium cations Pyranoanthocyanins Charge transfer Proton transfer Pump-probe spectroscopy

ABSTRACT

Pyranoflavylium cations are synthetic analogues of pyranoanthocyanin, colored pigments, formed from grape anthocyanins during the maturation of red wines. Studies of a series of monosubstituted pyranoflavylium cations, ranging from methoxy (PF+OMe) to cyano (PF+CN), have shown that they display fluorescence and form triplet states that sensitize singlet oxygen formation in acidified acetonitrile. In alcohol-water mixtures, they behave as photoacids, undergoing adiabatic excited state proton transfer (ESPT) to water on a picosecond timescale, as confirmed in this report by femtosecond pump-probe spectroscopy. In contrast, the corresponding dimethylamino substituted pyranoflavylium cation (PF+-NMe2) is virtually non-fluorescent under the same conditions and exhibits a long-wavelength absorption band that has been attributed to a charge-transfer (CT) transition. Indeed, pump-probe spectroscopy of PF+NMe2 in acidified acetonitrile shows ultrafast (<1 ps) formation of a CT state that decays back to the ground state with a 12-13 ps lifetime. In acidified methanol, the initial Franck-Condon CT state (ca. 3 ps lifetime) converts to a 13 ps lifetime CT state analogous to that in acetonitrile. In 50:50 ethanol:water and 30:70 methanol:water mixtures, PF+-NMe2 exhibits a short-lived (3-8 ps) initial CT state, an intermediate lifetime (30 ps) CT state and a much longer lived (130 ps) species attributed to a twisted intramolecular CT state. Thus, in addition to demonstrating that the photophysics of PF⁺-NMe₂ is dominated by CT rather than ESPT, pump-probe spectroscopy provides details of the solvent-dependent dynamics of the CT decay pathways.

1. Introduction

In recent years there has been growing interest in the use of naturally occurring plant dyes and their biomimetic analogs as substitutes for commercial pigments and food coloring additives [1–3]. Among the natural plant dyes, the anthocyanins are of particular interest due to the range of colors that they adopt combined with the lack of toxicity,

biodegradability and potential health benefits associated with their consumption [4–6]. Nonetheless, their practical applications are limited primarily to relatively acidic media due to the loss of their visible colors at neutral pH [7, 8]. Nucleophilic attack of water on the flavylium cation chromophore of the anthocyanin induces the loss of color, forming a near-colorless hemiketal, which occurs above ca. pH 3. The hemiketal can then undergo ring-opening tautomerization to form a near colorless

E-mail address: vullev@ucr.edu (V.I. Vullev).

https://doi.org/10.1016/j.jpap.2022.100110

^{*} Corresponding author.

¹ Equal contributions

² Present Address: College of Bioengineering, University of California, Berkeley, CA 94720, USA.

³ Present Address: Department of Chemistry, University of Texas at Austin, 105 E 24th St., Austin, TX 78712, USA.

⁴ Pesent Address: Division of Chemistry and Chemical Engineering, California Institute of Technology, Pasadena, CA 91125, USA.

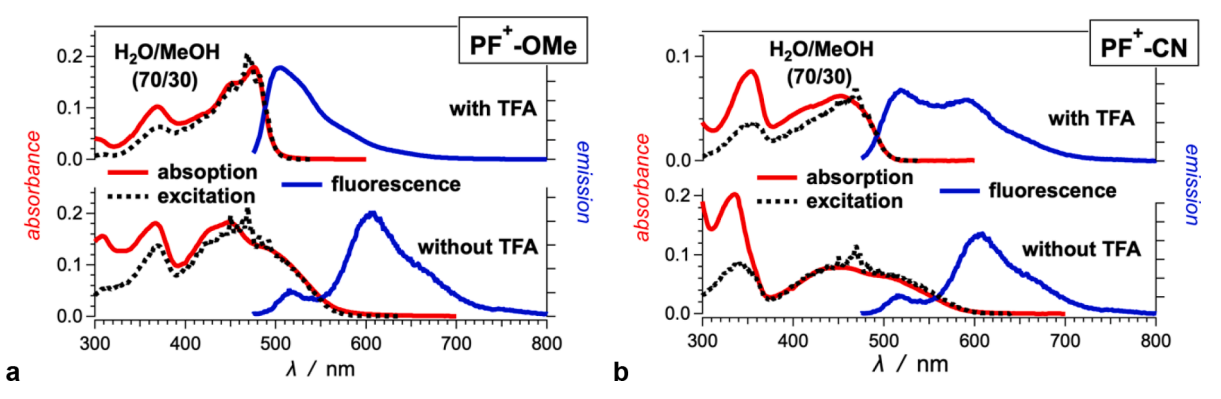


Fig. 1. Steady-state optical absorption, fluorescence and excitation spectra of (a) PF^+ -OMe and (b) PF^+ -CN for water/methanol (70/30, v/v) solution in the presence of 10 mM trifluoroacetic acid (TFA) and absence of TFA. For the fluorescence spectra, $\lambda_{ex} = 465$ nm; and for the excitation spectra, $\lambda_{em} = 550$ nm and 650 nm for presence and absence of TFA, respectively.

Table 1 Photophysical properties of **PF**⁺**-OMe** and **PF**⁺**-CN**.^a.

	solvent acidity	$arphi_f imes 10^3$ b	λ _{abs} /nm ^c	λ_{exc}/nm^{d}	λ _{fl} /nm ^e
PF ⁺ - OMe	10 mM TFA	250	369, 475	372, 470	507
	No TFA	30	365, 447, 494	369, 459	518,606
PF ⁺ -CN	10 mM TFA No TFA	30 4.0	352, 451 333, 450, 516	353, 462 340, 462	521, 587 518, 606

^aFor 30%_(V:V) CH₃OH in water.

chalcone with subsequent E/Z equilibration via isomerization of the chalcone.

In addition to chemical stability, photochemical stability is an important aspect of the long-term stability of the dye color and of their safety as coloring additives in food, cosmetics and other consumer products [8]. The chemistry and photophysics of anthocyanins mirror mostly those of synthetic flavylium cations, which possess the same basic chromophore [9–11]. Thus, fast sub-nanosecond adiabatic excited state proton transfer (ESPT) from the excited singlet state of the cationic form of anthocyanins to water results in the formation of the excited singlet state of the conjugate base, which decays to its ground state in less than a ns [11]. ESPT thus serves as an efficient (>99%) pathway for rapidly transforming the absorbed light energy into heat without producing potentially deleterious intermediates such as free radicals or excited triplet states that could potentially sensitize singlet oxygen formation [11].

In nature, the color of anthocyanins can be stabilized to higher pH by co-pigmentation [12], which involves either complexation with another colorless, electron-rich molecule [13] or chelation of a metal cation such as Al³⁺ [14]. A third mechanism of color stabilization, which occurs during the maturation of red wines, involves spontaneous chemical reactions of grape anthocyanins with other chemical components of the wine to form pyranoflavyliums (PFs) [15–17]. By virtue of an additional pyran ring (ring D, Chart 1) in their chemical structure, PFs are resistant to hydration and, as a result, their color is much less pH-dependent than that of anthocyanins [17]. Despite their improved stability, the PF dyes are susceptible to bleaching in alkaline media.

Certain blue and red plant tissues, such as grape skins or mature red wines, are a potential source for extracting a broad variety of PF

precursors [18, 19]. Although chemical modification of natural anthocyanins with vinylbenzene derivatives or molecules with enolizable keto groups, provides an alternative synthetic path to PFs [20], even after quite long reaction times the yields are low to moderate at best. As a consequence, the isolation and purification of naturally occurring PFs, along with scaling up viable higher-yield procedures for making them, are inherently challenging, and many aspects of the photophysics of these natural dyes are still unknown.

As in the case of anthocyanins, however, the essential features of the photophysics of **PFs** can presumably be inferred from those of synthetic pyranoflavylium cations that contain the same basic chromophore. The availability of relatively facile routes for the preparation and purification of substituted **PF**⁺ derivatives [21–26] has permitted a number of photophysical studies of these compounds [27–30]. Pyranoflavylium cations with a hydroxyl group are weak acids (with pK_a 's typically in the range of 3.5–4) in the ground state, but can undergo moderately fast ESPT in protic solvents with excited state pK_a * values of ca. 0.5 [29]. In acetonitrile solution acidified with trifluoroacetic acid (TFA) to suppress ESPT, excitation of pyranoflavylium cations was also found to result in intersystem crossing to the excited triplet state, with subsequent sensitized formation of singlet oxygen [31].

Experimental studies of a series of pyranoflavylium cations with substituents ranging from an electron-donating methoxy group (PF+-**OMe**) to an electron-withdrawing cyano group (**PF**⁺-**CN**) showed ESPT in protic solvents [28, 29], and fluorescence and triplet state formation in TFA-acidified acetonitrile [31]. On the other hand, two pyranoflavylium cations with pronouncedly strong electron-donating substituents, i.e., with three methoxy groups (PF+-(OMe)₃) or a dimethylamino group (PF⁺-NMe₂), on their rings B or E, were at best only weakly fluorescent and showed no triplet formation in acidified acetonitrile. The dimethylamino substituent is of particular interest because it provokes a pronounced bathochromic shift in the long-wavelength absorption band of flavylium [9, 10] and pyranoflavylium [23, 24, 27, 32] chromophores that is suggestive of a direct photoexcitation to a charge transfer (CT) state, rather than a localized absorption. Tests of a number of PF⁺ derivatives as the active chromophore in dve-sensitized solar cells revealed that PF⁺-NMe₂ offered the highest power-conversion efficiency among the compounds investigated [33-35].

Theoretical studies, employing *ab initio* quantum chemical calculations on this series of pyranoflavylium cations, corroborate the presence of a lowest twisted intramolecular charge transfer (TICT) excited singlet state for **PF**⁺-**NMe**₂ but not for **PF**⁺-**OMe** [27]. Because conventional steady-state and time-resolved fluorescence techniques proved to be uninformative with regard to the photophysics of **PF**⁺-**NMe**₂, in the present work we employed femtosecond pump-probe spectroscopy to obtain a detailed picture of the ultrafast processes governing the photophysics of **PF**⁺-**NMe**₂, as compared to those of **PF**⁺-**OMe** and **PF**⁺-**CN**,

^bFluorescence quantum yields determined using fluorescein in aqueous media (50 mM phosphate buffer, pH = 10) as a standard, λ_{ex} = 465 nm.

^cAbsorption maxima.

^dMaxima of the excitation spectra, in the presence of 10 mM TFA: $\lambda_{em}=550$ nm; and in the absence of TFA: $\lambda_{em}=650$ nm.

^eMaxima of the emission spectra, $\lambda_{ex} = 465$ nm.

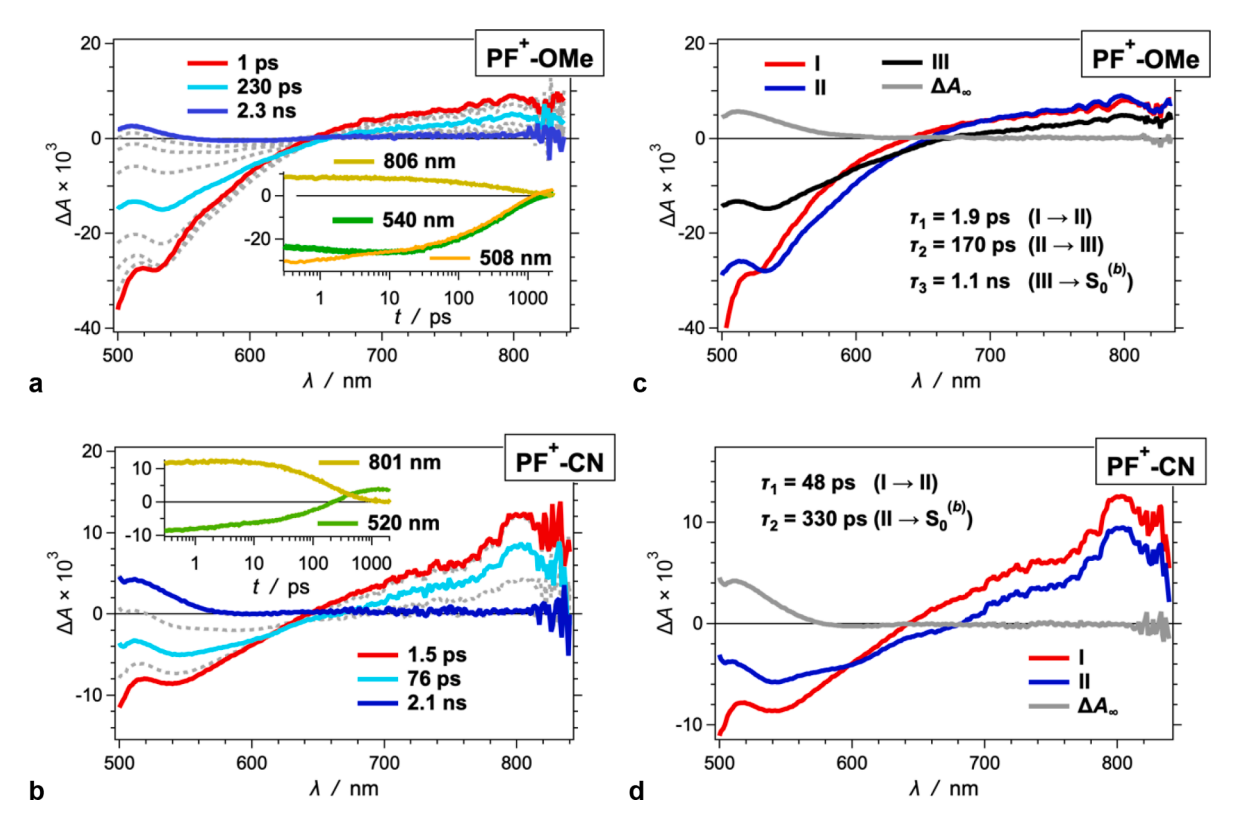


Fig. 2. Transient-absorption (TA) dynamics of (a,c) **PF**⁺-**OMe** and (b,d) **PF**⁺-**CN** for water/methanol (70/30, v/v) solution in the presence of 10 mM TFA. (a,b) TA spectra of **PF**⁺-**OMe** and **PF**⁺-**CN** recorded for different delay times, along with representative kinetic curves in the insets ($λ_{ex}$ = 465 nm; 4 μJ per pulse). The dashed gray lines represent the TA spectra recorded at intermediate times between those indicted in the legends. (c,d) Spectra showing the transitions associated with the time constants, $τ_b$, that the global fits produce, reconstructed from the amplitude distributions of the decay-associated difference spectra (DADS).

in acetonitrile and in polar protic solvents (methanol and alcohol-water mixtures).

2. Results and discussion

2.1. Absorption and fluorescence of the methoxy- and cyanofunctionalized pyranoflavyliums

Steady-state optical absorption spectra of the methoxy- and cyanofunctionalized compounds PF^+ -OMe and PF^+ -CN in the presence and absence of trifluoroacetic acid (TFA) show the effects of proton transfer from the hydroxyl group to the solvent. In the presence of TFA, the optical absorption spectra show a strong band around 460 nm, due to the $S_0 \rightarrow S_1$ transition of the cationic acid form of the dyes, PF^+ -OMe and PF^+ -CN (Fig. 1). In the absence of TFA, an additional shoulder also appears in the spectral region from about 550 – 600 nm (Fig. 1, Table 1), corresponding to the long-wavelength absorption band of the conjugate base form (Scheme 1).

As is the case with other hydroxyaromatic compounds, these pyranoflavylium cations are more acidic in the singlet excited state (pK_a^* for ESPT of 0.66 and 0.37 for the methoxy and cyano derivatives, respectively) than in the ground state (pK_a of 3.8 and 3.7, respectively) [29]. Thus, the steady-state emission spectra show fluorescence signals from both the excited acid and base forms of the PFs (Fig. 1). For the methoxy-substituted PF, the emission of the photoacid, ${}^1PF^+$ -OMe*, dominates the fluorescence spectrum in the presence of TFA (Fig. 1a). In contrast, the emission spectrum of the cyano derivative exhibits intense fluorescence of the base, 1PF -CN*, at about 590 nm, in addition to the 520-nm band of the cationic form, ${}^1PF^+$ -CN* (Fig. 1b, Scheme 1). In the absence of TFA, both PFs show predominant fluorescence from their deprotonated forms, along with less intense photoacid emission at around 520 nm (Fig. 1). The fluorescence quantum yields, Φ_6 of the acid

form in the presence of TFA are about an order of magnitude larger than those for the net emission quantum yield (acid plus base form) in the absence of added TFA (Table 1), consistent with the smaller Φ_f of the conjugate base forms.

2.2. Pump-probe spectroscopy of the methoxy- and cyano-functionalized pyranoflavyliums

The femtosecond pump-probe transient-absorption (TA) spectra of PF⁺-OMe and PF⁺-CN in the presence of TFA (Fig. 2a,b) are dominated in the visible region by the ground-state bleach (B) and stimulated emission (SE) of the cationic form. The broad weak band in the red and near-infrared (NIR) region, i.e., at $\lambda \gtrsim 650$ nm (Fig. 2a,b) is attributed to $S_1 \rightarrow S_n$ transitions. These transients decay on a sub-nanosecond time scale, resulting in the emergence of TA bands at around 500 to 600 nm due to long-lived species (Fig. 2a,b), i.e., species that persist for times much longer than the 3-ns dynamic range of our pump-probe system. Multiexponential global-fit (GF) analysis of the PF⁺-OMe TA dynamics reveals an initial fast relaxation, with $\tau_1 \approx 2$ ps, resulting in a slight SE bathochromic shift (Fig. 2c). This initial decay is followed by a decrease in the amplitudes of the SE signal and the 700-nm TA, with $\tau_2 \approx 150$ ps (Fig. 2c). Finally, the SE and TA bands decay with $\tau_3 \approx 1$ ns to form the long-lived transient with absorption extending to about 600 nm (Fig. 2c). We attribute τ_1 to relaxation of the Franck-Condon (FC) excited state and τ_2 to the adiabatic excited state proton transfer (ESPT) process, i.e., ${}^1\!PF^+\text{-}OMe^*{\to}{}^1\!PF\text{-}OMe^*$. The value of τ_3 is in good agreement with the fluorescence lifetime of the singlet excited state of the base [29, 36]; its decay to the ground state (Scheme 2) is thus responsible for the residual long-lived absorption in the TA (Fig. 2a,c), which matches well that of the base in the ground-state absorption spectra (Fig. 1a).

The TA dynamics of PF+-CN reveal a similar excited-state behavior, but with time constants that are about three times smaller than those for

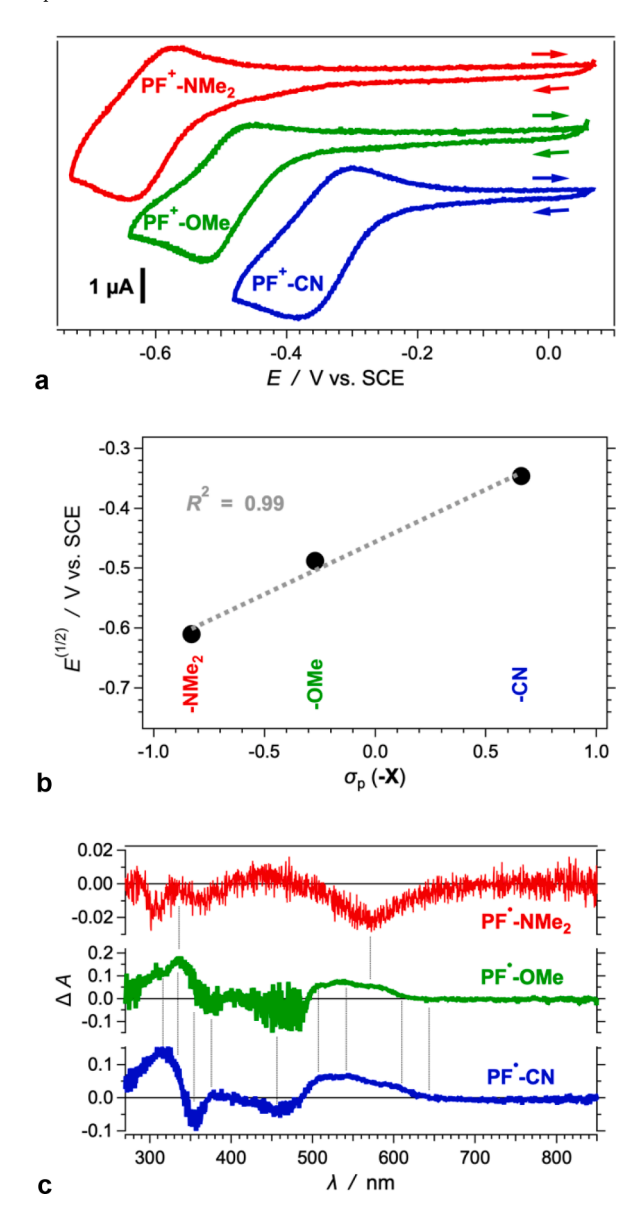


Fig. 3. Electrochemical characterization of the PF^+ -X dyes. (a) Cyclic voltammograms showing the reduction of the PF^+ -X dyes for acetonitrile in the presence of 25 mM (n-C₄H₉)₄NPF₆ and 1 mM TFA, scan rates, v=50 mV s^{-1} [45–48]. (b) Correlation between the half-wave reduction potentials, $E^{(1/2)}$ of the PF^+ -X dyes and the Hammett constant, σ_p , of the substituent -X on the ring E (Chart 1) [49]. (c) Difference spectra showing the changes in the absorption, ΔA , recorded around the peaks of the cathodic waves during the scans. The spectra are ascribed to the reduced forms, i.e., the radicals PF^* -X, of the dyes [50–52]. While an increase in sample concentration increases the current density and the concentration of the radicals produced at the electrode surfaces, it also increases the optical density of the solution, making the signal-to-noise ratios unfeasibly small, as the differential spectrum of the methoxy derivative shows in the range between 440 and 485 nm.

PF⁺-**OMe** (Fig. 2d). The value of τ_2 of about 0.3 ns matches well the fluorescence lifetime of the excited-state base, 1 **PF-CN*** [29]. The intermediate lifetimes τ_2 derived from the present single exponential global fits can only be compared qualitatively to the multiexponential kinetic parameters for the ESPT process determined from an analysis of time-resolved fluorescence spectroscopic measurements on the acid and base forms of these two PF derivatives.

2.3. Electrochemical reduction of the pyranoflavylium cations

The positive charge on the condensed rings makes pyranoflavyliums strong electron acceptors. The cyclic voltammograms of the three $\mathbf{PF}^+\mathbf{X}$ dyes show quasi-reversible behavior, indicating that their reduced neutral radical forms are relatively stable (Fig. 3a). The reduction potentials range between about -0.6 and -0.35 V vs. SCE, which is on par with those of some of the best organic electron acceptors and photo-oxidants, such as perylenediimides, quinones and nitroaromatics [37–44]. The electron-withdrawing and donating strength of the substituent X attached to ring E (Chart 1) exerts a relatively strong influence on the reduction potentials, inducing a variation of about 0.3 V (Fig. 3b).

The differential absorption spectra of the reduced forms of the methoxy and the cyano derivatives, i.e., the corresponding neutral radicals **PF*-OMe** and **PF*-CN**, exhibit a broad band around 550 nm and a sharper one in the UV region (Fig. 3c). Between 350 and 500 nm, ΔA varies between positive and negative values as a result of the overlap of the absorption of the radicals with the bleach due to depletion of the ground-state absorption of the pyranoflavylium cations (Fig. 3c). The change from a methoxy to a cyano group causes a 15-nm hypsochromic shift of the UV band. However, the 550-nm band appears to be quite similar for **PF*-OMe** and **PF*-CN**, suggesting that it is relatively insensitive to the electron-withdrawing or donating strength of the substituent on ring E.

Reduction of $\mathbf{PF^+}$ - $\mathbf{NMe_2}$ induced a bleach, rather than a positive ΔA band, in the region between 500 and 600 nm (Fig. 3c). This suggests that the absorption band of $\mathbf{PF^-}$ - $\mathbf{NMe_2}$ has a smaller molar extinction coefficient than the overlapping ground-state absorption band of $\mathbf{PF^+}$ - $\mathbf{NMe_2}$, which is consistent with the spectral features of $\mathbf{PF^-}$ - \mathbf{OMe} and $\mathbf{PF^-}$ - \mathbf{CN} . This indicates that the absorption band at around 550 nm of the \mathbf{PF} radicals is practically unaffected by the substituent on the peripheral rings.

2.4. Absorption and fluorescence of the dimethylamino pyranoflavylium

As noted above, the cationic form of the PF chromophore is an excellent electron acceptor and photooxidant (Fig. 3), while aminophenyl groups are good electron donors. Thus, the dimethylamino substituted PF+-NMe2 is expected to exhibit intramolecular charge transfer (ICT) transitions in its absorption spectra. Indeed, both in the presence and absence of TFA, the steady-state absorption spectra of PF⁺- NMe_2 reveal a broad intense band between about 500 and 600 nm (Fig. 4). This new feature sets PF⁺-NMe₂ apart from the cyano and methoxy PFs (Figs. 1 and 4), and is consistent with a direct transition to an excited state with predominant CT character, i.e., $S_0^{(a)} \rightarrow S_1^{(CT)}$ (Scheme 2), in concordance with the results of ab initio quantum chemical calculations. [27]. For acidified media, the 550-nm band dominates the visible region of the absorption spectra of PF⁺-NMe₂ (Fig. 4). For protic solvents in the absence of TFA, on the other hand, a shoulder at 520 nm and a band around 450 nm emerge (Fig. 4b,c), consistent with a contribution from the absorption of the ground-state base, PF-NMe₂. Indeed, the ground-state pK_a of the OH group of **PF**⁺-**NMe**₂ of 3.9 [33] is only modestly higher than those of the other two PFs, which show the presence of partial proton transfer to the protic solvent under the same conditions. The hypsochromic shoulder on the 550-nm CT band and the band at 450 nm, which disappear in acidic media, are thus attributed, respectively, to the $S_0^{(b)} \rightarrow S_1^{(b)}$ transition of the base (Scheme 2) and to an optical transition to upper excited states of the base, i.e., $S_0^{(b)} \rightarrow S_n^{(b)}$. This assignment is consistent with the observation that, in the aprotic solvent acetonitrile, the 450-nm band is absent regardless of the acidity of the medium (Fig. 4d), reflecting the fact that the ground-state equilibrium is completely shifted to the cationic form PF+-NMe₂ (S₀^(a), Scheme 2) due to the poor proton-accepting character of this solvent.

The fluorescence spectra of PF^+ - NMe_2 in protic solvents reveal a major emission band at around 650 nm that, at first glance, might

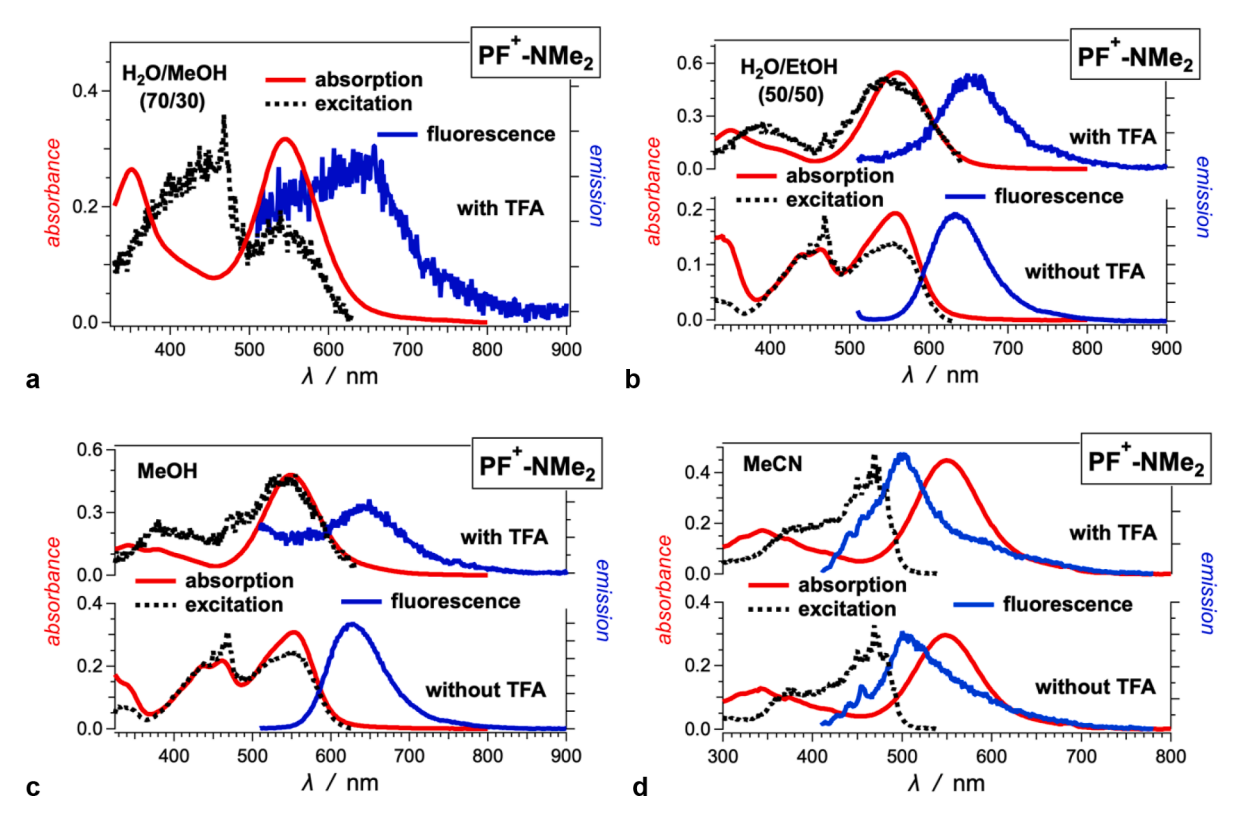


Fig. 4. Steady-state optical absorption, fluorescence and excitation spectra of **PF**⁺-**NMe**₂ for (a) water/methanol (70/30, v/v) solution mixture, (b) water/ethanol (50/50, v/v) solution mixture, (c) methanol and (d) acetonitrile, in the presence and absence of TFA. For the fluorescence spectra, (a,b,c) $\lambda_{ex} = 500$ nm (d) $\lambda_{ex} = 400$ nm; and for the excitation spectra, (a,b,c) $\lambda_{em} = 640$ nm and (d) $\lambda_{em} = 550$ nm.

Table 2
Photophysical properties of PF⁺-NMe₂.

solvent	solvent acidity	$\mathop{\varphi_{\!f}}_{\rm a}\times 10^3$	$_{_{ m b}}^{\lambda_{abs}}/{ m nm}$	$_{ m c}^{\lambda_{exc}/nm}$	λ_{fl}/nm		
H ₂ O/MeOH ^e (70/30)	10 mM TFA	0.38	545	444, 542	630		
H ₂ O/EtOH	10 mM TFA	0.77	560	546	653		
(50/50)	No TFA	11	460, 556	468, 553	634		
MeOH	10 mM TFA	0.66	549	540	642		
	No TFA	6.9	460, 551	468, 550	628		
MeCN ^f	10 mM TFA	0.96	550	468	500		
	No TFA	1.5	549	470	507		

^aFluorescence quantum yields determined using eosin Y dissolved in ethanol as a standard; $\lambda_{ex} = 500$ nm, unless otherwise noted.

550 nm; and for the emission spectra, $\lambda_{ex} = 400$ nm.

appear to be the mirror image of the 500–600-nm CT absorption band (Fig. 4a-c). In the absence of added TFA in protic solvents, the net fluorescence quantum efficiencies, Φ_f , of $\mathbf{PF^+}$ - $\mathbf{NMe_2}$ are comparable to those of $\mathbf{PF^+}$ - \mathbf{OMe} and $\mathbf{PF^+}$ - \mathbf{CN} (Tables 1 and 2). The addition of TFA, however, decreases the Φ_f of $\mathbf{PF^+}$ - $\mathbf{NMe_2}$ by more than an order of magnitude (Table 2), a trend that is opposite to that observed for the other two \mathbf{PFs} (Table 1). This trend indicates that the observed fluorescence in the absence of added TFA is dominated by the emission of the excited base, $^1\mathbf{PF-NMe_2}^*$, that is more strongly fluorescent than the CT state of the acid form of $\mathbf{PF^+}$ - $\mathbf{NMe_2}$. This conclusion is confirmed by the comparison of the absorption and fluorescence excitation spectra in

protic solvents in the absence of TFA. In the region between 500 and 600 nm, the relative amplitudes in the excitation spectra are distinct from those in the absorption spectra, with a more pronounced shoulder at 520 nm and a clear excitation band at 450 nm (Fig. 4b,c). In fact, the 550-nm band in the excitation spectra points to the presence of two overlapping fluorescence signals in non-acidified protic media, one from the more fluorescent excited base, $S_1^{(b)} \rightarrow S_0^{(b)}$, and the other from the much more weakly fluorescent CT state, $S_1^{(CT)} \rightarrow S_0^{(a)}$, of the cation (Scheme 2) Thus, the small amount of conjugate base in equilibrium with the cationic form may be responsible for the somewhat higher contribution of the spectral region between 400 and 500 nm in the excitation spectra in protic media compared to the ground-state absorption spectra under these same conditions (Fig. 4a-c).

The absorption spectra of PF+-NMe2 in acetonitrile display the 550nm CT band but not the 450-nm band (Fig. 4d), suggesting that the ground-state base is not present in detectable amounts in this solvent. The lack of a well-defined fluorescence band between 600 and 700 nm suggests that the CT state is essentially non-fluorescent in acetonitrile (Fig. 4d). In strongly acidic media, the protonation of the dimethylamine $\,$ might also potentially produce the dye dication, PF+-N+HMe2 (Scheme 2), which has an absorption band around 450 nm [25] that overlaps with the $S_0^{(b)} \rightarrow S_n^{(b)}$ absorption of the base. In aqueous solution, the reported pK_a of the dye dication, $PF^+-N^+HMe_2$, is below 1 [33], so that the amount of dication present should be negligible in protic solvents containing 0.01 M added TFA. On the other hand, in the very weakly basic aprotic solvent acetonitrile, the relative changes in the acidity of TFA and the basicity of the dimethylamine substituent [53, 54] are apparently sufficient to form a small amount of the dication, as indicated by the distinct excitation and emission spectra for this solvent (Fig. 4d). These spectra are more consistent with a trace amount of highly fluorescent dication than with emission from the conjugate base. The presence of the same emission in the absence of added TFA, which might argue against this assignment, is probably due to the synthetic protocol,

^bAbsorption maxima.

^cMaxima of the excitation spectra, $\lambda_{em}=640$ nm, unless otherwise noted.

^dMaxima of the emission spectra, $\lambda_{ex} = 500$ nm, unlessen otherwise noted.

^ePF⁺-NMe₂ is not soluble in water/methanol solution unless it is acidified. ^fFor the acetonitrile samples, coumarin 151 in ethanol is used as a standard for the fluorescence quantum yield, $\lambda_{ex} = 400$ nm; for the excitation spectra, $\lambda_{em} = 400$ nm;

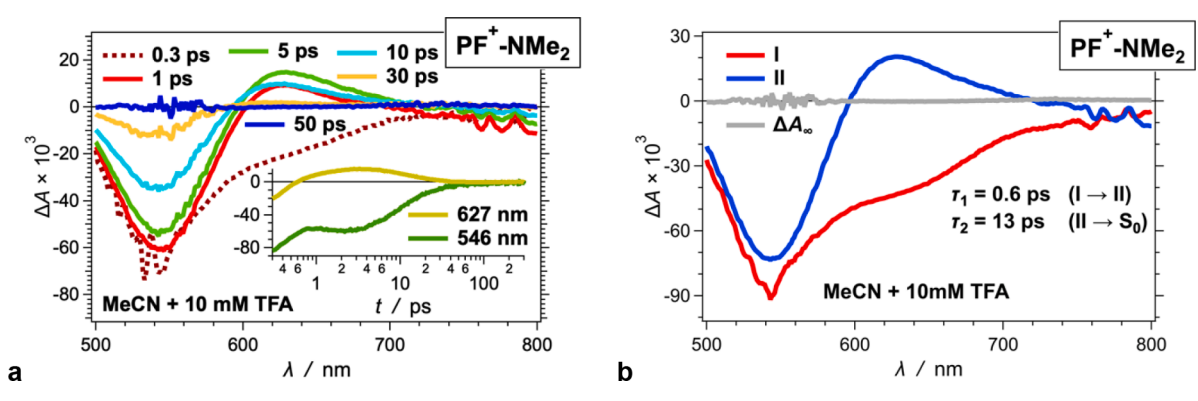


Fig. 5. TA dynamics of PF^+ -NMe₂ for acetonitrile in the presence of 10 mM TFA. (a) TA spectra of PF^+ - NMe₂ recorded for different delay times, along with representative kinetic curves in the insets ($λ_{ex} = 465$ nm; 4 μJ per pulse). (b) Spectra showing the transitions associated with the time constants, $τ_b$ that the global fits produce, reconstructed from the amplitude distributions of DADS. For the TA dynamics in the presence of 0.1 mM TFA, 1 mM TFA and 100 mM TFA, see the Supplementary Data (Appendix A).

which includes a final washing with cold, HCl-acidified water that could result in a small amount of the dication in the reaction product.

2.5. Transient-absorption dynamics of the dimethylamino pyranoflavylium cation

The TA spectroscopic studies focused on acidified solvents where, as outlined above, the mono-cation, $\mathbf{PF^+}$ - $\mathbf{NMe_2}$, is the preponderant species present. In acidified acetonitrile the excitation of $\mathbf{PF^+}$ - $\mathbf{NMe_2}$ results in an initial ground-state bleach, peaking at ca. 540 nm due to overlap with the SE that appears as a broad shoulder at ca. 640 nm (Fig. 5, S1 and S2). The sub-picosecond decay of the SE signal, which removes its overlap with the ground-state bleach and shifts the negative ΔA maximum from 540-nm to 550 nm, accompanies a rise of a TA band around 620, ascribed to a CT excited state, and a SE band in the near infrared (NIR) beyond 700 nm. The lack of such detectable NIR emission in the steady-state fluorescence spectra indicates that the CT state absorbing at 620 nm manifests only very weak NIR fluorescence.

The transition to this CT state is in effect an electron transfer from the highest occupied molecular orbital of the dimethylanilino E ring (Chart 1) to the photoexcited **PF**⁺ core or, equivalently, of a hole-shift process that displaces the positive charge from the **PF**⁺ core to the dimethylanilino ring [55–58]. Biaryl linkers, such as that between rings D and E (Chart 1), provide sufficient electronic coupling to mediate adiabatic hole shifts with sub-picosecond rates [59, 60]. The 620-nm TA band of the CT state, the 550-nm bleach and the NIR SE band decay in 12–13 ps to a zero baseline throughout the entire spectral region probed. Some participation of the dication (**PF**⁺-**N**⁺**HMe**₂, Scheme 2) cannot be ruled out. Nonetheless, the fact that the rate of formation of the CT state, its subsequent decay and the TA spectra are insensitive to added TFA concentration from 0.1 to 100 mM (Fig. 5a, S1) suggests that, if present, the dication, **PF**⁺-**N**⁺**HMe**₂, has little or no effect on the TA spectroscopic results.

In TFA-acidified methanol, the TA dynamics reveal further details about the excited-state transitions of $\mathbf{PF^+}$ -NMe₂ (Fig. 6a,d). The ground-state bleach and the SE signal dominate the initial TA spectrum of $\mathbf{PF^+}$ -NMe₂. Within the 0.2-ps instrument-response time, photoexcitation of $\mathbf{PF^+}$ -NMe₂ leads to: (1) an intense 600-nm negative-amplitude band, consistent with SE from the acid, $S_1^{(a)} \rightarrow S_0^{(a)}$; (2) a well-defined shoulder at around 550 nm from the overlap with the ground-state bleach; and (3) a broad weak positive TA band in the near infrared spectral region, characteristic of $S_1 \rightarrow S_n$ optical transitions of the acid of these dyes (compare Spectra I in Figs. 2b and 6d). Thus, in less than 200 fs, the upper excited state, formed by the 400-nm excitation, relaxes to the locally excited acid state, i.e., $S_n^{(a)} \rightarrow S_1^{(a)}$. An ultrafast (0.34 ps) transition reduces the amplitude of the negative ΔA signals by more than a factor of two, producing a TA spectrum with two overlapping bands at

550 and 640 nm (Spectrum II, Fig. 6d). The former band matches the ground-state CT absorption and the latter the CT fluorescence observed in the steady-state emission spectra of $\mathbf{PF^+}$ - $\mathbf{NMe_2}$ in acidified methanol (Fig. 4, Table 2). This femtosecond CT step is too fast for large-amplitude nuclear rearrangements. Therefore, the structure of this CT state has to be similar to (but not exactly the same as) that of the ground state and the Franck-Condon excited states, warranting its $\mathbf{S_1}^{(\mathrm{FC}'\mathrm{CT})}$ designation (Scheme 2).

A ca. 3 ps transition leads to the growth of the 620-nm band and a shift of the weak SE signal to the NIR region (Spectrum III, Fig. 6d), which are the features of the CT state observed in acetonitrile. These spectral changes (II \rightarrow III, Fig. 6d) therefore represent a $S_1^{(\text{FC-CT})} \rightarrow S_1^{(\text{CT})}$ transition, involving further localization of the positive charge on the dimethylaminophenyl donor and the radical on the PF condensed rings. The presence of the NIR SE suggests that this CT state, $S_1^{(CT)}$, does not have a completely orthogonal twisted intramolecular charge transfer geometry, which would be expected to be a dark state. The time required for the $S_1^{(FC'CT)} \rightarrow S_1^{(CT)}$ transition of just over 3 ps (II \rightarrow III, Fig. 6d) is much slower than in acetonitrile, but probably still too fast to allow substantial dihedral twisting of the dimethylanilinophenyl ring. Hence, it is more compatible with a slower solvent reorganization in methanol relative to acetonitrile in response to the large CT-induced shift in the distribution of the positive charge. In methanol, this solvent-reorganized CT state decays with a 13-ps lifetime (Fig. 6d), identical within experimental error to that in acetonitrile.

Adding water to alcohols increases the polarity of the solvating media. With a dielectric constant of about 55 [61], a 50:50 (v:v) mixture of ethanol and water is more polar than methanol. The water present in the mixture also acts as a better proton acceptor and proton donor than the alcohols. Upon photoexcitation, the TA spectrum of $PF^+\text{-NMe}_2$, in a TFA-acidified 50:50 water-ethanol mixture shows the 550-nm ground-state bleach and the 640-nm shoulder due to SE from the $S_1^{(FC'CT')}$ state (Fig. 6b,e), followed by a 3 ps growth of the 620-nm TA band of the $S_1^{(CT')}$ state and its NIR SE emission (Fig. 6e). The $S_1^{(CT')}$ state lives ca. 2-fold longer than in either methanol or acetonitrile, decaying with a lifetime of 29 ps to a species characterized by a much weaker, longer-lived bleach at 540 nm that decays in 130 ps back to the baseline.

The relatively weak bleach in the 500–600-nm region is consistent with the spectrum of the reduced radical form of this dye (Fig. 3c). Concurrently, a radical cation localized on the dimethylaminophenyl moiety should absorb at around 465 nm [62], outside the spectral range of the white-light generator of our pump-probe system. Therefore, the long-lived bleach is consistent with a TICT state, S₁^(TICT), with sufficient orthogonality to diminish the electronic coupling between the reduced **PF** and oxidized dimethylaminophenyl moieties to the point that SE becomes unobservable.

The 540-nm bleach is also a good match for the ground state base,

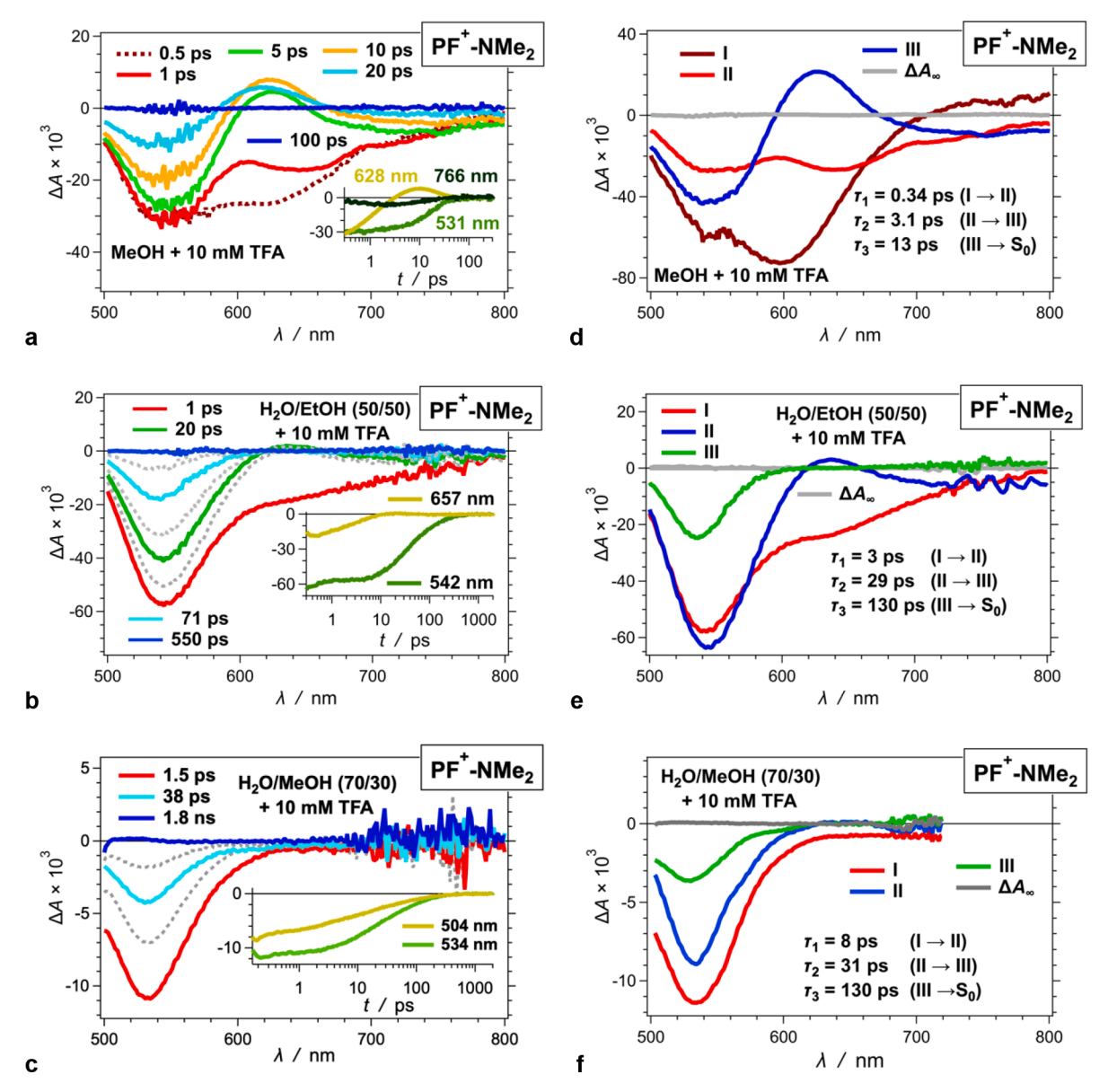


Fig. 6. TA dynamics of PF⁺-NMe₂ for (a,d) methanol (b,e) water/ethanol (50/50, v/v) solution mixture, and (c,f) water/methanol (70/30, v/v) solution mixture, in the presence of 10 mM TFA. (a-c) TA spectra of PF⁺-NMe₂ recorded for different delay times, along with representative kinetic curves in the insets (λ_{ex} = 465 nm; 4 μJ per pulse). The dashed gray lines represent the TA spectra recorded at intermediate times between those indicted in the legends. (d-f) Spectra showing the transitions associated with the time constants, τ_b that the global fits produce, reconstructed from the amplitude distributions of DADS. While for all samples the optical density at λ_{ex} was kept between 0.4 and 0.6 for 2-mm cuvettes, for the water/methanol media, $A(\lambda_{ex})$ was around 0.1 because of insufficient solubility. Lowering sample concentrations decreases the $-\Delta A$ amplitude of the 535-nm band and the signal-to-noise ratio in the near infrared region around 750 nm.

considering that the molar extinction coefficient of the $S_0^{(b)} \rightarrow S_1^{(b)}$ transition is smaller than that of the $S_0^{(a)} \rightarrow S_1^{(FC'CT)}$ transition. The hole shift in the TICT state, however, should abolish its photoacidity. Furthermore, a lifetime of 130 ps is too short for a bimolecular protonation process of a ground-state base. Therefore, the most plausible attribution of this last species is a polar-solvent-stabilized TICT state, consisting of a PF radical of the dye largely electronically decoupled from an orthogonal oxidized dimethylaminonophenyl moiety.

Increasing the polarity of the water-containing solvent, while altering the shapes of the TA spectra at wavelengths longer than about 600 nm, does not considerably affect the excited-state dynamics. The dielectric constant of 30% methanol in water is about 67 [63]. Instead of a well-defined SE band (or a shoulder) accompanying the 530-nm bleach formed upon photoexcitation, the SE appears as a broad weak signal extending from the bathochromic edge of the bleach to the NIR spectral region (Fig. 6c, f). The tiny amplitude of this SE signal is consistent with

the smaller fluorescence quantum yield, i.e., about 4×10^{-4} , and longer SE lifetime, i.e., 8 ps, of PF^+ -NMe₂ in acidified water–methanol medium in comparison with those for the other solvents with TFA (Table 2, Fig. 5, 6). This spectrum (Spectrum I, Fig. 6f) is ascribed to a state with a CT character formed within the instrument response time, but its structure is different than that of the pseudo FC CT states, $S_1^{(FC^*CT)}$, observed in the other solvent media. Because the time for the formation of this CT state is too short for significant nuclear rearrangements, this suggests that the ground state, $S_0^{(a)}$, of PF^+ -NMe₂ may have a somewhat different equilibrium geometry (i.e., torsion angles) in predominantly aqueous solvents compared to the other more organic-rich solvent media examined.

The SE signals decay in 8 ps, accompanied by a slight decrease in the bleach amplitude and the appearance of a shoulder at about 560 nm (Spectrum II, Fig. 6f). In another 30 ps, the amplitude of the bleach decreases by a factor of 2.5 and undergoes a 5-nm hypsochromic shift

acid forms

base forms

Scheme 1. Acid-base equilibria of ground- and excited-states pyranoflavyliums.

that decays to ground state in 130 ps (Spectrum III, Fig. 6f). The 130 ps lifetime is consistent with a TICT state whose PF radical-like absorption overlaps with the somewhat more intense bleach of the ground-state absorption of the dye (Fig. 3c). The spectrum of the intermediate $S_1^{(CT)}$ state (Spectrum II, Fig. 6f) is also different from that of the $S_1^{(CT)}$ states observed in the other solvent media because it lacks the 620-nm absorption band and the NIR SE characteristic of this state in other solvents. In this regard, in methanol and water-ethanol, the $S_1^{(FC'CT)} \rightarrow S_1^{(CT)}$ transition involves an increase in the bleach amplitude (II→III on Fig. 6d, and I→II on Fig. 6e). A bathochromic shift of a TA band from the 550-nm region to 620 nm accompanying the $S_1^{(\text{FC'CT})} \rightarrow S_1^{(\text{CT})}$ transition due, e.g., to a change in the dihedral angle between the donor and the acceptor, can account for the observed TA spectral trends. If the transition increased the oscillator strength without provoking the bathochromic shift, however, the result would be a decrease in the amplitude of the 550-nm bleach band, which is precisely what is observed in the TA dynamics of PF+-NMe2 in acidified water-methanol.

It is common for chromophores with biaryl linkers between electron donor and acceptor moieties forming S₁ states with a pronounced CT character to undergo dihedral twists [64]. Inherently, increasing the dihedral angle in such twisted CT states decreases the overlap between the natural-transition orbitals involved in their radiative deactivation. Some twisted CT states, thus, are fluorescent with increased Stokes' shifts, while others are dark, i.e., their emission is practically undetectable [64]. That is, dyes comprising biaryl-linked donor and acceptor units can form partially twisted fluorescent CT states that evolve into dark TICT structures [43, 44]. As computational studies show, among a number of PF⁺ dyes, only PF⁺-NMe₂ exhibits an increase in the dihedral angle between rings D and E upon optimization of the geometry of its first singlet excited state. For the gas phase, the dihedral angle of the optimized S_0 state of **PF**⁺-**NMe**₂ is 9.4° and of the optimized S_1 state it is 33.2° [27]. In contrast, the dihedral angles between rings D and E of the optimized S_0 and S_1 states of PF^+ -OMe and PF^+ -CN are practically the same [27]. These trends are consistent with the TA dynamics of **PF**⁺-**NMe**₂ that completely differs from that of the other dyes, justifying the assignment of some of the transients to twisted excited states with a pronounced CT character.

3. Conclusions

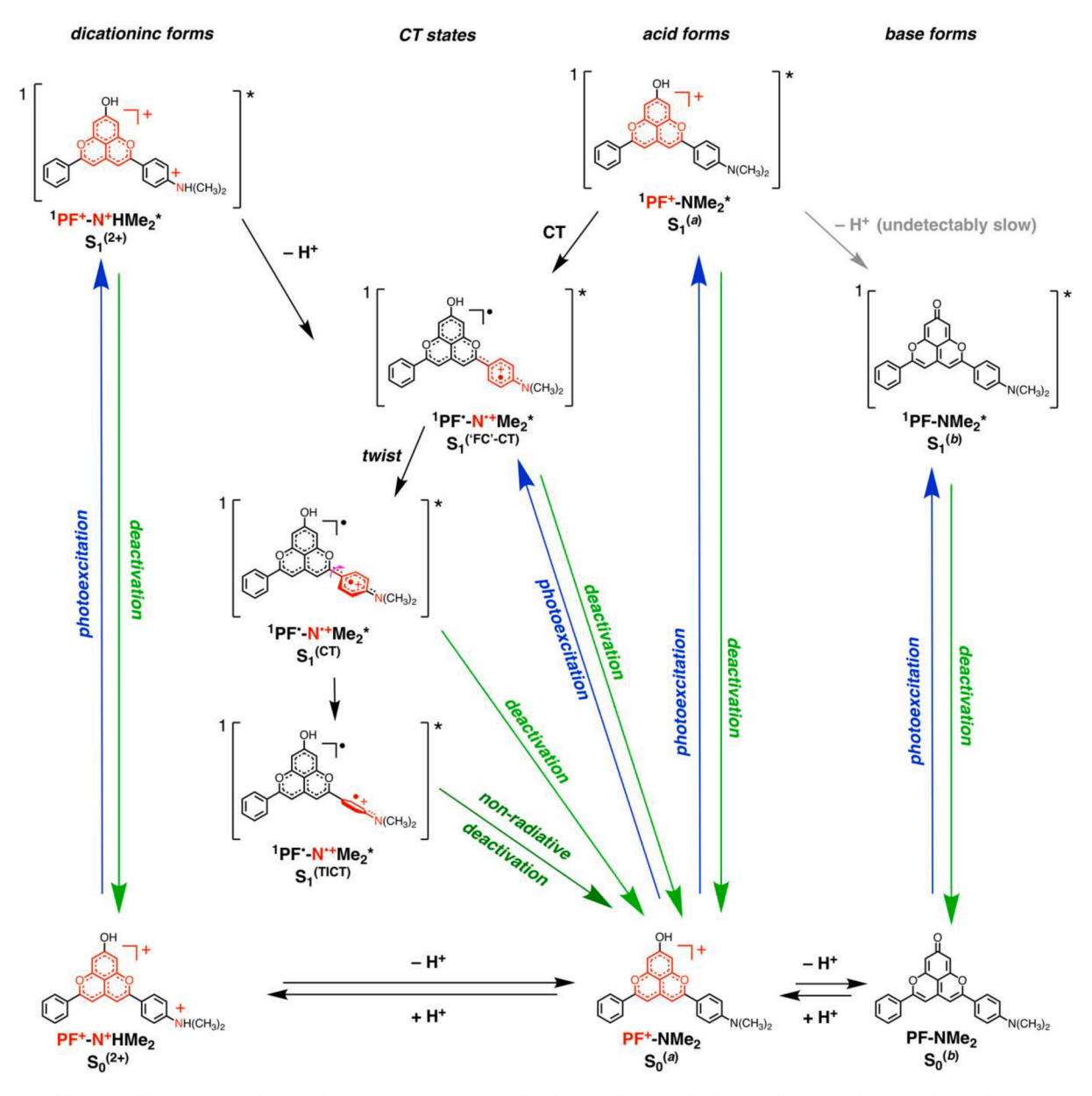
Femtosecond pump-probe spectroscopy demonstrates the importance of ESPT as the major decay pathway of PF⁺-OMe and PF⁺-CN in methanol/water mixtures, in agreement with time-resolved fluorescence results for these compounds. In the case of PF+-NMe2, pumpprobe spectroscopy confirms that the lack of significant fluorescence can be ascribed to ultrafast formation of short-lived CT states that precludes ESPT. The excited state dynamics of PF+-NMe2 are solventdependent and point to the presence of several intermediate CT states along the pathway back to the ground state. The initially formed CT species is the one most strongly affected by solvent reorganization, with a lifetime that increases from less than a ps in acetonitrile to 3-8 ps in alcohol-water mixtures. This is consistent with the large shift in the positive charge distribution of the molecule accompanying excitation, from a hole delocalized over most of the pyranoflavylium chromophore to a more localized hole on the dimethylaminophenyl moiety. In acidified acetonitrile or methanol, the initial CT state converts to a CT state that is relatively short-lived (12-13 ps) due to fast back electrontransfer. In much more polar alcohol:water media, where selective solvation might also play a role, this latter CT state not only lives longer (30 ps), but also evolves to a much longer lived (130 ps) TICT state prior to undergoing back electron-transfer. Together with their straightforward synthesis and relatively low reduction potentials, pyranoflavylium cations are thus potentially interesting as acceptor moieties in photoinduced electron transfer systems.

Appendix A. Supplementary Data

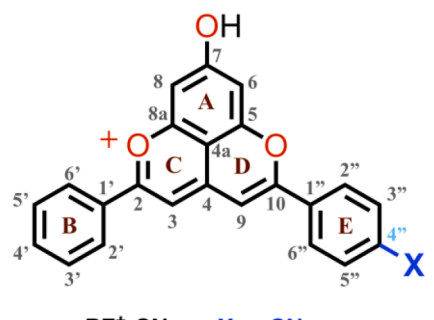
Supplementary data, containing experimental details and additional spectra associated with this article, can be found in the online version at:

Declaration of Competing Interest

The authors declare that they have no known competing financial interests or personal relationships that could have appeared to influence the work reported in this paper.



Scheme 2. Acid-base equilibria and excited-states charge transfer for a pyranoflavylium with a strongly electron-donating substituent that is also a proton acceptor. a



PF⁺-CN: -X = -CNPF⁺-OMe: $-X = -OCH_3$ PF⁺-NMe₂: $-X = -N(CH_3)_2$

Chart 1. Structure of biomimetic pyranoflavyliums.

Acknowledgements

The authors thank the U.S.A. National Science Foundation (grant number CHE 1800602 and AGEP supplement fellowship for J.A.C.), the American Chemical Society Petroleum Research Fund (grant number 60651-ND4), and the U.S.A. National Institutes of Health, National Eye Institute (grant R01 EY027440) for funding this work. V.I.V. thanks the Fulbright Program for supporting his work at Universidade de Saõ Paulo, Saõ Paulo, Brazil. F. H. Q., C. P. S. and G. T. M. S. thank the CNPq and CAPES (Finance code 001), respectively, for fellowships and NAP-PhotoTech, INCT-Catálise (CNPq 465454/2014–3 and 444061/2018–5), and CNPq (FHQ Universal grant 408181/2016–3) for funding.

Supplementary materials

Supplementary material associated with this article can be found, in the online version, at doi:10.1016/j.jpap.2022.100110.

References

- [1] S. Saxena, A.S.M. Raja, Natural dyes: sources, chemistry, application and sustainability issues, in: S. Muthu (Ed.), Roadmap to Sustainable Textiles and Clothing, Textile Science and Clothing Technology, Springer, Singapore, 2014.
- [2] M.J. Shetty, P.R. Geethalekshmi, C. Mini, Natural pigments as potential food colourants: a review, Trends Biosci. 10 (2017) 4057–4064.
- [3] S.J. Ranaweera, A.A.L.T. Ampemohotti, U.S.P.R. Arachchige, Advantages and considerations for the applications of natural food pigments in the food industry, J. Res. Technol. Eng. 1 (2020) 8–15.
- [4] M. Horbowicz, R. Kosson, A. Grzesiuk, H. Dębski, Anthocyanins of fruits and vegetables-their occurrence, analysis and role in human nutrition, Veg. Crop. Res. Bull. 68 (2008) 5–22.
- [5] J.A. He, M.M. Giusti, Anthocyanins: natural colorants with health-promoting properties, Annu. Rev. Food. Sci. T. 1 (2010) 163–187.
- [6] C.D. Kay, G. Pereira-Caro, I.A. Ludwig, M.N. Clifford, A. Crozier, Anthocyanins and flavanones are more bioavailable than previously perceived: a review of recent evidence, Annu. Rev. Food. Sci. T. 8 (2017) 155–180.
- [7] A. Castaneda-Ovando, M.D. Pacheco-Hernandez, M.E. Paez-Hernandez, J. A. Rodriguez, C.A. Galan-Vidal, Chemical studies of anthocyanins: a review, Food Chem. 113 (2009) 859–871.
- [8] F.H. Quina, E.L. Bastos, Chemistry inspired by the colors of fruits, flowers and wine, An. Acad. Bras. Cienc. 90 (2018) 681–695.
- [9] F. Pina, M.J. Melo, C.A.T. Laia, A.J. Parola, J.C. Lima, Chemistry and applications of flavylium compounds: a handful of colours, Chem. Soc. Rev. 41 (2012) 869–908.
- [10] F. Pina, J. Oliveira, V. de Freitas, Anthocyanins and derivatives are more than flavylium cations, Tetrahedron 71 (2015) 3107–3114.
- [11] F.H. Quina, P.F. Moreira, C. Vautier-Giongo, D. Rettori, R.F. Rodrigues, A. A. Freitas, P.F. Silva, A.L. Macanita, Photochemistry of anthocyanins and their biological role in plant tissues, Pure Appl. Chem. 81 (2009) 1687–1694.
- [12] P. Trouillas, J.C. Sancho-Garcia, V. De Freitas, J. Gierschner, M. Otyepka, O. Dangles, Stabilizing and modulating color by copigmentation: insights from review theory and experiment, Chem. Rev. 116 (2016) 4937–4982.
- [13] P.F. da Silva, J.C. Lima, A.A. Freitas, K. Shimizu, A.L. Macanita, F.H. Quina, Charge-transfer complexation as a general phenomenon in the copigmentation of anthocyanins, J. Phys. Chem. A 109 (2005) 7329–7338.
- [14] K. Yoshida, M. Mori, T. Kondo, Blue flower color development by anthocyanins: from chemical structure to cell physiology, Nat. Prod. Rep. 26 (2009) 884–915.
- [15] A. Marquez, M.P. Serratosa, J. Merida, Pyranoanthocyanin derived pigments in wine: structure and formation during winemaking, J. Chem. 2013 (2013).
- [16] J. Oliveira, N. Mateus, V. de Freitas, Previous and recent advances in pyranoanthocyanins equilibria in aqueous solution, Dyes Pigm. 100 (2014) 190–200
- [17] H. Oliveira, N. Wu, Q. Zhang, J.Y. Wang, J. Oliveira, V. de Freitas, N. Mateus, J. R. He, I. Fernandes, Bioavailability studies and anticancer properties of malvidin based anthocyanins, pyranoanthocyanins and non-oxonium derivatives, Food Funct. 7 (2016) 2462–2468.
- [18] J. He, A.R.F. Carvalho, N. Mateus, V. De Freitas, Spectral features and stability of oligomeric pyranoanthocyanin-flavanol pigments isolated from red wines, J. Agric. Food Chem. 58 (2010) 9249–9258.
- [19] J.T. Bozic, N. Curko, K.K. Ganic, L. Butinar, A. Albreht, I. Vovk, D. Korte, B. M. Vodopivec, Synthesis of pyranoanthocyanins from Pinot Noir grape skin extract using fermentation with high pyranoanthocyanin producing yeasts and model wine storage as potential approaches in the production of stable natural food colorants, Eur. Food Res. Technol. 246 (2020) 1141–1152.
- [20] S. Gomez-Alonso, D. Blanco-Vega, M. Gomez, I. Hermosin-Gutierrez, Synthesis, isolation, structure elucidation, and color properties of 10-acetyl-pyranoanthocyanins, J. Agric. Food Chem. 60 (2012) 12210–12223.
- [21] M. Schwarz, P. Winterhalter, A novel synthetic route to substituted pyranoanthocyanins with unique colour properties, Tetrahedron Lett. 44 (2003) 7583–7587.
- [22] S. Chassaing, G. Isorez-Mahler, M. Kueny-Stotz, R. Brouillard, Aged red wine pigments as a source of inspiration for organic synthesis the cases of the colorstable pyranoflavylium and flavylium-(4->8)-flavan chrornophores, Tetrahedron 71 (2015) 3066–3078.
- [23] J. Oliveira, A. Fernandes, V. de Freitas, Synthesis and structural characterization by LC-MS and NMR of a new semi-natural blue amino-based pyranoanthocyanin compound, Tetrahedron Lett. 57 (2016) 1277–1281.
- [24] J. Oliveira, P. Araujo, A. Fernandes, N.F. Bras, N. Mateus, F. Pina, V. de Freitas, Influence of the structural features of amino-based pyranoanthocyanins on their acid-base equilibria in aqueous solutions, Dyes Pigm. 141 (2017) 479–486.
- [25] J.L.C. Sousa, V. Gomes, N. Mateus, F. Pina, V. de Freitas, L. Cruz, Synthesis and equilibrium multistate of new pyrano-3-deoxyanthocyanin-type pigments in aqueous solutions, Tetrahedron 73 (2017) 6021–6030.
- [26] C.P. da Silva, R.M. Pioli, L. Liu, S.S. Zheng, M.J. Zhang, G.T.D. Silva, V.M. T. Carneiro, F.H. Quina, Improved synthesis of analogues of red wine pyranoanthocyanin pigments, Acs Omega 3 (2018) 954–960.
- [27] F. Siddique, C.P. Silva, G.T.M. Silva, H. Lischka, F.H. Quina, A.J.A. Aquino, The electronic transitions of analogs of red wine pyranoanthocyanin pigments, Photoch. Photobio. Sci. 18 (2019) 45–53.
- [28] J. Wang, F. Siddique, A.A. Freitas, C.P. Silva, G.T.M. Silva, F.H. Quina, H. Lischka, A.J.A. Aquino, A computational study of the ground and excited state acidities of synthetic analogs of red wine pyranoanthocyanins, Theor. Chem. Acc. 139 (2020).
- [29] A.A. Freitas, C.P. Silva, G.T.M. Silva, A.L. Macanita, F.H. Quina, Ground- and excited-state acidity of analogs of red wine pyranoanthocyanins, Photochem. Photobiol. 94 (2018) 1086–1091.

- [30] C.P. Silva, G.T.M. Silva, T.D. Costa, V.M.T. Carneiro, F. Siddique, A.J.A. Aquino, A. A. Freitas, J.A. Clark, E.M. Espinoza, V.I. Vullev, F.H. Quina, Chromophores inspired by the colors of fruit, flowers and wine, Pure Appl. Chem. 92 (2020) 255–263.
- [31] G.T.M. Silva, S.S. Thomas, C.P. Silva, J.C. Schlothauer, M.S. Baptista, A.A. Freitas, C. Bohne, F.H. Quina, Triplet excited states and singlet oxygen production by analogs of red wine pyranoanthocyanins, Photochem. Photobiol. 95 (2019) 176–182.
- [32] J. Oliveira, P. Araujo, A. Fernandes, N. Mateus, V. de Freitas, Synthesis and structural characterization of amino-based pyranoanthocyanins with extended electronic delocalization, Synlett 27 (2016) 2459–2462.
- [33] A.L. Pinto, H. Cruz, J. Oliveira, P. Araujo, L. Cruz, V. Gomes, C.P. Silva, G.T. M. Silva, T. Mateus, G. Calogero, V. de Freitas, F.H. Quina, F. Pina, A.J. Parola, J. C. Lima, Dye-sensitized solar cells based on dimethylamino-pi-bridge-pyranoanthocyanin dyes, Sol. Energy 206 (2020) 188–199.
- [34] X. Shi, Y. Li, L. Wang, Two novel mono-hydroxyl pyranoanthocyanidins bearing dimethylamino substituent(s) for dye-sensitized solar cell, J. Mol. Struct., (2021) 132055
- [35] C.M. Santos, B. Gomes, L.M. Goncalves, J. Oliveira, S. Rocha, M. Coelho, J. A. Rodrigues, V. Freitas, H. Aguilar, Pyranoflavylium derivatives extracted from wine grape as photosensitizers in solar cells, J. Brazil. Chem. Soc. 25 (2014) 1029–1035.
- [36] A.A. Freitas, C.P. Silva, G.T.M. Silva, A.L. Macanita, F.H. Quina, From vine to wine: photophysics of a pyranoflavylium analog of red wine pyranoanthocyanins, Pure Appl. Chem. 89 (2017) 1761–1767.
- [37] S.K. Lee, Y. Zu, A. Herrmann, Y. Geerts, K. Muellen, A.J. Bard, Electrochemistry, spectroscopy and electrogenerated chemiluminescence of perylene, terrylene, and quaterrylene diimides in aprotic solution, J. Am. Chem. Soc. 121 (1999) 3513–3520.
- [38] R. Orłowski, J.A. Clark, J.B. Derr, E.M. Espinoza, M.F. Mayther, O. Staszewska-Krajewska, J.R. Winkler, H. Jędrzejewska, A. Szumna, H.B. Gray, V.I. Vullev, D. T. Gryko, Role of intramolecular hydrogen bonds in promoting electron flow through amino acid and oligopeptide conjugates, Proc. Natl. Acad. Sci. U. S. A. 118 (2021), e2026462118.
- [39] D. Bao, S. Ramu, A. Contreras, S. Upadhyayula, J.M. Vasquez, G. Beran, V.I. Vullev, Electrochemical reduction of quinones: interfacing experiment and theory for defining effective radii of redox moieties, J. Phys. Chem. B 114 (2010) 14467–14479.
- [40] K. Rybicka-Jasinska, E.M. Espinoza, J.A. Clark, J.B. Derr, G. Carlos, M. Morales, M. K. Billones, O. O Mari, H. Agren, G.V. Baryshnikov, V.I. Vullev, Making nitronaphthalene fluoresce, J. Phys. Chem. Lett. 12 (2021) 10295–10303.
- [41] E.M. Espinoza, B. Xia, N. Darabedian, J.M. Larsen, V. Nunez, D. Bao, J.T. Mac, F. Botero, M. Wurch, F. Zhou, V.I. Vullev, Nitropyrene photoprobes: making them, and what are they good for?, Eur. J. Org. Chem., (2016) 343–356.
- [42] G. Jones II, L.N. Lu, V. Vullev, D. Gosztola, S. Greenfield, M. Wasielewski, Photoactive peptides. 6. Photoinduced electron transfer for pyrenesulfonamide conjugates of tryptophan-containing peptides. Mitigation of fluoroprobe behavior in N-terminal labeling experiments, Bioorg. Med. Chem. Lett. 5 (1995) 2385–2390.
- [43] Y.M. Poronik, G.V. Baryshnikov, I. Deperasinska, E.M. Espinoza, J.A. Clark, H. Agren, D.T. Gryko, V.I. Vullev, Deciphering the unusual fluorescence in weakly coupled bis-nitro-pyrrolo[3,2-b]pyrroles, Commun. Chem. 3 (2020) 190.
- [44] B. Sadowski, M. Kaliszewska, Y.M. Poronik, M. Czichy, P. Janasik, M. Banasiewicz, D. Mierzwa, W. Gadomski, T.D. Lohrey, J.A. Clark, M. Lapkowski, B. Kozankiewicz, V.I. Vullev, A.L. Sobolewski, P. Piatkowski, D.T. Gryko, Potent strategy towards strongly emissive nitroaromatics through a weakly electron-deficient core, Chem. Sci. 12 (2021) 14039–14049.
- [45] E.M. Espinoza, J.A. Clark, J. Soliman, J.B. Derr, M. Morales, V.I. Vullev, Practical aspects of cyclic voltammetry: how to estimate reduction potentials when irreversibility prevails, J. Electrochem. Soc. 166 (2019) H3175–H3187.
- [46] E.M. Espinoza, J.M. Larsen, V.I. Vullev, What makes oxidized N-acylanthranilamides stable? J. Phys. Chem. Lett. 7 (2016) 758–764.
- [47] D. Bao, B. Millare, W. Xia, B.G. Steyer, A.A. Gerasimenko, A. Ferreira, A. Contreras, V.I. Vullev, Electrochemical oxidation of ferrocene: a strong dependence on the concentration of the supporting electrolyte for nonpolar solvents, J. Phys. Chem. A 113 (2009) 1259–1267.
- [48] O. O'Mari, V.I. Vullev, Electrochemical analysis in charge-transfer science: the devil in the details, Curr. Opin. Electrochem. 31 (2022), 100862.
- [49] C. Hansch, A. Leo, R.W. Taft, A survey of hammett substituent constants and resonance and field parameters, Chem. Rev. 91 (1991) 165–195.
- [50] D. Bao, S. Upadhyayula, J.M. Larsen, B. Xia, B. Georgieva, V. Nunez, E. M. Espinoza, J.D. Hartman, M. Wurch, A. Chang, C.-K. Lin, J. Larkin, K. Vasquez, G.J.O. Beran, V.I. Vullev, Dipole-mediated rectification of intramolecular photoinduced charge separation and charge recombination, J. Am. Chem. Soc. 136 (2014) 12966–12973.
- [51] H.G. Ryu, M.F. Mayther, J. Tamayo, C. Azarias, E.M. Espinoza, M. Banasiewicz, L. G. Lukasiewicz, Y.M. Poronik, A. Jezewski, J. Clark, J.B. Derr, K.H. Ahn, D. T. Gryko, D. Jacquemin, V.I. Vullev, Bidirectional solvatofluorochromism of a pyrrolo[3,2-b]pyrrole-diketopyrrolopyrrole hybrid, J. Phys. Chem. C 122 (2018) 13424–13434.
- [52] A. Purc, E.M. Espinoza, R. Nazir, J.J. Romero, K. Skonieczny, A. Jeżewski, J. M. Larsen, D.T. Gryko, V.I. Vullev, Gating that suppresses charge recombination—the role of mono-n-arylated diketopyrrolopyrrole, J. Am. Chem. Soc. 138 (2016) 12826–12832.
- [53] K. Sarmini, E. Kenndler, Ionization constants of weak acids and bases in organic solvents, J. Biochem. Bioph. Meth. 38 (1999) 123–137.

- [54] J.T. Muckerman, J.H. Skone, M. Ning, Y. Wasada-Tsutsui, Toward the accurate calculation of pKa values in water and acetonitrile, Biochim. Biophys. Acta, Bioenerg. 1827 (2013) 882–891.
- [55] J.B. Derr, J. Tamayo, J.A. Clark, M. Morales, M.F. Mayther, E.M. Espinoza, K. Rybicka-Jasinska, V.I. Vullev, Multifaceted aspects of charge transfer, Phys. Chem. Chem. Phys. 22 (2020) 21583–21629.
- [56] M. Krzeszewski, E.M. Espinoza, C. Cervinka, J.B. Derr, J.A. Clark, D. Borchardt, G. J.O. Beran, D.T. Gryko, V.I. Vullev, Dipole effects on electron transfer are enormous, Angew. Chem. Int. Ed. 57 (2018) 12365–12369.
- [57] G. Jones II, D. Yan, J. Hu, J. Wan, B. Xia, V.I. Vulley, Photoinduced electron transfer in arylacridinium conjugates in a solid glass matrix, J. Phys. Chem. B 111 (2007) 6921–6929.
- [58] J. Hu, B. Xia, D. Bao, A. Ferreira, J. Wan, G. Jones, V.I. Vullev, Long-lived photogenerated states of α-oligothiophene-acridinium dyads have triplet character, J. Phys. Chem. A 113 (2009) 3096–3107.
- [59] G. Jones II, D.-.X. Yan, D.J. Gosztola, S.R. Greenfield, M.R. Wasielewski, Photoinduced charge migration in the picosecond regime for thianthrene-linked acridinium ions, J. Am. Chem. Soc. 121 (1999) 11016–11017.
- [60] G. Jones II, M.S. Farahat, S.R. Greenfield, D.J. Gosztola, M.R. Wasielewski, Ultrafast photoinduced charge-shift reactions in electron donor-acceptor 9-arylacridinium ions, Chem. Phys. Lett. 229 (1994) 40–46.
- [61] J. Wyman, The dielectric constant of mixtures of ethyl alcohol and water from-5 to 40(o), J. Am. Chem. Soc. 53 (1931) 3292–3301.
- [62] A. Maroz, R. Hermann, S. Naumov, O. Brede, Ionization of aniline and its N-methyl and N-phenyl substituted derivatives by (Free) electron transfer to n-butyl chloride parent radical cations, J. Phys. Chem. A 109 (2005) 4690–4696.
- [63] P.S. Albright, L.J. Gosting, Dielectric constants of the methanol water system from 5-degrees to 55-degrees, J. Am. Chem. Soc. 68 (1946) 1061–1063.
- [64] Z.R. Grabowski, K. Rotkiewicz, W. Rettig, Structural changes accompanying intramolecular electron transfer: focus on twisted intramolecular charge-transfer states and structures, Chem. Rev. 103 (2003) 3899–4031.